Applied Catalysis B: Environmental 176–177 (2015) 338–346

Contents lists available at ScienceDirect

Applied Catalysis B: Environmental

journal homepage: www.elsevier.com/locate/apcatb

A novel Ce–Ta mixed oxide catalyst for the selective catalytic reduction of NO_x with NH_3

Tao Zhang, Ruiyang Qu, Wenkang Su, Junhua Li*

State Key Joint Laboratory of Environment Simulation and Pollution Control, School of Environment, Tsinghua University, Beijing 100084, China

ARTICLE INFO

Article history:
Received 5 January 2015
Received in revised form 10 April 2015
Accepted 13 April 2015
Available online 14 April 2015

Keywords:
NH_3-SCR
Ta addition
Chemisorbed oxygen species
Surface acid sites
NO_x adsorbed species

ABSTRACT

A series of novel $Ce_aTa_bO_x$ catalysts prepared by a co-precipitation method was investigated on selective catalytic reduction (SCR) of NO_x with NH_3. It was found that the $Ce_1Ta_1O_x$ catalyst showed excellent activity, N_2 selectivity and strong resistance to H_2O and SO_2 through a relatively wide temperature range. The $Ce_aTa_bO_x$ catalysts were characterized using XRD, BET, XPS, H_2-TPR, NH_3-TPD, NO + O_2-TPD and in situ DRIFTS. The characterization results indicated that Ta addition could increase the BET surface area and the surface acidity of the catalysts, lead to the appearance of higher levels of Ce^{3+} and chemisorbed oxygen species, influence the reducibility of the catalysts, and promote the presence of nitrite and nitrate species. According to the in situ DRIFTS investigations, the reactivity of surface-adsorbed NH_3 and NO_x species depended on the temperature.

1. Introduction

Nitrogen oxides (NO_x) emitted from automobile exhaust gas and the industrial combustion of fossil fuels could lead to acid rain, photochemical smog, ozone depletion, and greenhouse effects and endanger human health [1]. The selective catalytic reduction (SCR) with NH_3 has been proven to be the most effective method for controlling NO_x emissions. V_2O_5-WO_3 (MoO_3)/TiO_2-based SCR catalysts have been commercially used for stationary source applications since the 1970s [2]. However, there are still some inevitable problems existing in the V-based catalyst, such as the high working temperature and the toxicity of vanadium species. Therefore, it is important to develop vanadium-free SCR catalysts for the removal of NO_x.

Cerium oxides are widely accepted as promising candidates due to their outstanding oxygen storage-release capacity and excellent redox properties in the NH_3-SCR reaction. However, pure CeO_x oxides usually have poor NH_3-SCR activity. In most cases, doping improves the catalytic performance compared to that of the undoped host oxide by increasing the conversion, the selectivity, or the area per gram of catalyst. Recently, many types of doped Ce-based catalysts were reported, such as Ce–Mn [3], Ce–P [4], Ce–Ti [5], Ce–W [6,7], Ce–Mo [8], Ce–Nb [9], Ce–W–Ti [10], Ce–Cu–Ti oxides [11], and Ce–Mn–Ti [12]. These Ce-based composite oxide catalysts are more attractive than single oxide catalysts because other metal elements can promote the catalytic properties of CeO_x. Meanwhile, the onset of electronic effects and/or the formation of composite phases have been proposed to be responsible for the improvement in catalytic activity. For the NH_3–SCR reaction, a dual-site mechanism, including an acid site and a redox site, has also been proposed [2].

Up to now, comparatively fewer investigations of Ta-based catalysts for the selective catalytic reduction of NO_x have been reported. In this study, highly efficient $Ce_aTa_bO_x$ binary oxide catalysts were prepared using a co-precipitation method, and the catalysts showed excellent catalytic performance. The effects of tantalum on the surface properties of the catalyst were also studied using N_2 physisorption, X-ray diffraction (XRD), X-ray photoelectron spectroscopy (XPS), temperature-programmed reduction (H_2-TPR), NH_3 temperature-programmed desorption (NH_3-TPD), NO + O_2 temperature-programmed desorption (NO + O_2-TPD) and in situ diffuse reflectance infrared Fourier transform spectroscopy (in situ DRIFTS). Finally, the reactivity of surface-adsorbed NH_3 and NO_x species on the $Ce_1Ta_1O_x$ catalyst was investigated using in situ DRIFTS.

2. Experimental

2.1. Catalyst preparation and activity test

The $Ce_aTa_bO_x$ catalysts with different atomic ratios of Ce and Ta were prepared by a co-precipitation method. Typically,

* Corresponding author. Tel.: +86 10 62771093; fax: +86 10 62771093.
E-mail address: lijunhua@tsinghua.edu.cn (J. Li).

http://dx.doi.org/10.1016/j.apcatb.2015.04.023
0926-3373/

$NH_3{\cdot}H_2O$ solution (25%) was dropped into a stoichiometric solution of $Ce(NO_3)_3{\cdot}6H_2O$ and $TaCl_5$ with continuous stirring. Then, the suspension was aged in air for 2 h at room temperature and atmospheric pressure. The resultant precipitates were dried at 100 °C overnight and subsequently calcined at 500 °C for 5 h under air at ambient conditions. The mixed oxides were denoted as $Ce_aTa_bO_x$, where a/b represents the molar ratio of Ce/Ta on the basis of the amount of $Ce(NO_3)_3{\cdot}6H_2O$ and $TaCl_5$ used. For comparison, CeO_x and Ta_2O_5 were also prepared by a similar precipitation method.

A fixed-bed quartz flow reactor (I.D. = 6 mm) was used for the SCR activity tests at atmospheric pressure. The reaction conditions were controlled as follows: 500 ppm NO, 500 ppm NH_3, 5% O_2, 5.5% H_2O (when used), 150 ppm SO_2 (when used), and N_2 as balance gas. 0.1 g catalysts of 40–60 mesh were used for evaluation. The total flow rate was 200 mL min^{-1}, and the gas hourly space velocity (GHSV) was 120,000 mL g^{-1} h^{-1}. Concentrations of NO, NH_3, NO_2 and N_2O were monitored by an FTIR spectrometer (MKS, MultiGas 2030HS). The data for steady-state activity of catalysts were recorded after about 30 min at each temperature. The NO_x conversion, N_2 selectivity and the pseudo-first order rate constant (k) [13] were calculated according to the following equations:

$$NO_x\ \text{Conversion} = \frac{[NO_x]_{inlet} - [NO_x]_{outlet}}{[NO_x]_{inlet}} \times 100\% \quad (1)$$

$$N_2\ \text{Selectivity} = \left(1 - \frac{2[N_2O]_{outlet}}{[NO_x]_{inlet} + [NH_3]_{inlet} - [NO_x]_{outlet} - [NH_3]_{outlet}}\right) \times 100\% \quad (2)$$

$$k = -\frac{F}{W}\ln(1-x) \quad (3)$$

where F is the total flow rate (cm^3 s^{-1}), W is the weight of the catalyst (g) and x is the relative NO_x conversion.

2.2. Physical and chemical characterization

Powder XRD patterns were recorded on a powder X-ray diffractometer (Rigaku, D/max-2200, Japan) equipped with Cu Kα (λ = 0.15405 nm) radiation at a rate 10°/min over a 2θ range of 10–80°. The diffraction lines were identified by matching them with reference patterns in the JCPDS database.

The N_2 sorption isotherm was measured at 77 K using a micromeritics ASAP 2020 instrument in static mode. The samples were degassed at 300 °C for 4 h prior to the measurements. The specific surface area was calculated from the adsorption branch in the P/P_0 range from 0.05–0.30 using the Brunauer–Emmett–Teller (BET) equation. Pore volumes and average pore diameters were determined by the Barrett–Joyner–Halenda (BJH) method from the desorption branches of the isotherms.

X-ray photoelectron spectroscopy (XPS) results of the catalysts were recorded on an ESCALab220i-XL electron spectrometer from VG Scientific using 300 W Mg Ka radiation. All the binding energies were calibrated using the C 1s peak (BE = 284.8 eV) as an internal standard.

Temperature programmed reduction with H_2 (H_2-TPR) experiments were performed on a chemisorption analyzer (Micromeritics, ChemiSorb 2720 TPx). The samples in a quartz reactor were pretreated at 300 °C in Ar for 1 h and cooled down to the room temperature. Then H_2-TPR was performed in 10% H_2/Ar gas flow of 50 mL/min at a heating rate of 10 °C min^{-1}. To quantify the total amount of H_2 consumed during these experiments, CuO was used as a calibration reference.

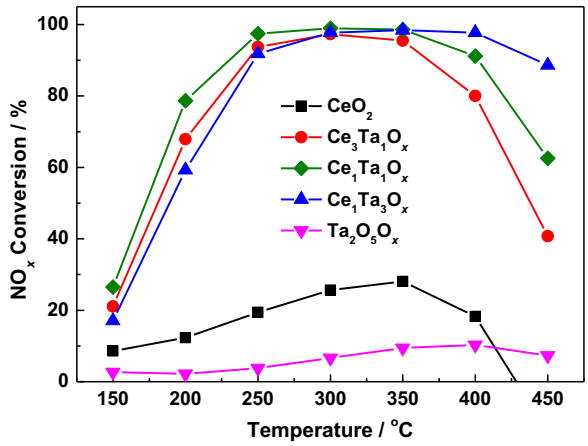

Fig. 1. NO_x conversion as a function of temperature in the NH_3–SCR reaction over $Ce_aTa_bO_x$ series catalysts. Reaction conditions: [NO] = [NH_3] = 500 ppm, [O_2] = 5%, N_2 balance, total flow rate 200 mL min^{-1} and GHSV = 120,000 mL g^{-1} h^{-1}.

Temperature programmed desorption (TPD) of NH_3 or NO + O_2 was carried out using a FTIR spectrometer (MKS, MultiGas 2030HS) to detect different nitrogen-containing species including NH_3, NO and NO_2. The samples were pretreated at 350 °C in N_2 flow (200 mL min^{-1}) for 1 h. Afterward, the samples were cooled down to 100 °C and saturated with NH_3 or NO + O_2 until adsorption equilibrium was reached, followed by N_2 purging at the same temperature for 2 h. The desorption of nitrogen-containing species was performed in the range of 100–500 °C using a ramp of 10 °C min^{-1}.

In situ DRIFTS experiments were performed on an FTIR spectrometer (Nicolet NEXUS 6700) equipped with a smart collector and an MCT/A detector. Prior to each experiment, the catalyst was pretreated at 350 °C for 1 h in N_2 at a flow of 100 mL min^{-1}. The DRIFTS spectra were recorded by accumulating 32 scans with a resolution of 4 cm^{-1}.

3. Results and discussion

3.1. NH_3–SCR performance

Fig. 1 shows the NO_x conversion as a function of temperature over $Ce_aTa_bO_x$ catalysts in the NH_3–SCR reaction. Without Ta doping, the pristine CeO_x exhibited poor NO_x conversion in the whole temperature range. When the Ce/Ta molar ratio was 3:1, the catalytic activity of $Ce_3Ta_1O_x$ catalyst was greatly improved, with more than 80% NO_x conversion from 250 to 400 °C. This result indicates that a synergistic effect for the NH_3–SCR reaction might exist between Ce and Ta species. For the $Ce_1Ta_1O_x$ catalyst, the reaction activity was further improved in the whole test temperature range. When the Ce/Ta molar ratio was decreased to 1:3, the operation temperature window shifted toward higher temperatures. The pristine Ta_2O_5 sample also showed poor SCR activity, indicating again that the coexistence of Ce and Ta species is very important for the promotion of SCR activity.

As shown in Fig. 2, the N_2 selectivity of the CeO_x catalyst decreased noticeably above 300 °C with quite a large amount of N_2O being formed. However, nearly 100% N_2 selectivity was obtained over $Ce_aTa_bO_x$ catalysts in the whole temperature range investigated, indicating that the introduction of Ta species to the catalyst could suppress the unselective catalytic oxidation of NH_3 to N_2O or NO at high temperatures. These catalysts were further characterized to discuss the structure–activity relationship in the NH_3–SCR reaction.

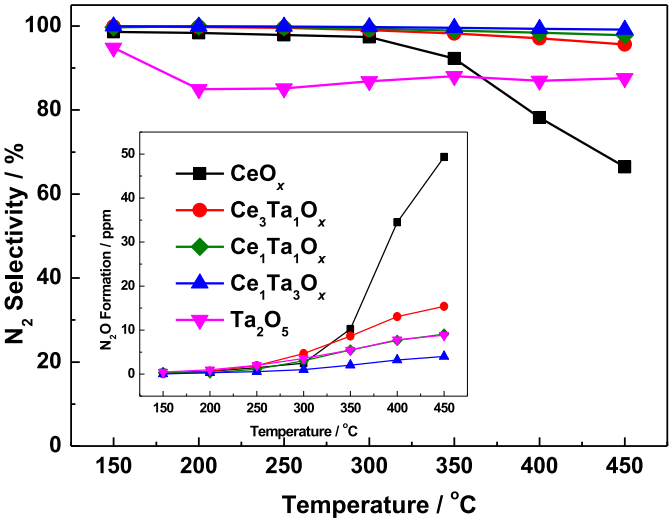

Fig. 2. N_2 selectivity and N_2O formation as a function of temperature in the NH_3–SCR reaction over $Ce_aTa_bO_x$ series catalysts. Reaction condition: [NH_3] = [NO] = 500 ppm, [O_2] = 5%, N_2 balance, total flow rate 200 mL min^{-1} and GHSV = 120,000 mL g^{-1} h^{-1}.

3.2. Effect of H_2O and SO_2

Because the H_2O and SO_2 in the combustion exhaust often lead to the deactivation of the SCR catalyst, the SCR activity in the presence of H_2O and SO_2 needs to be considered. The effect of H_2O and SO_2 on the SCR activity of $Ce_1Ta_1O_x$ catalyst at 300 °C was investigated and the results are shown in Fig. 3. When 5.5% H_2O was introduced into the stream at 300 °C, the value of NO_x conversion decreased slightly and remained above 90% during the activity test for 12 h. This result indicates that water vapor inhibits the catalytic activity slightly at 300 °C, which may be attributed to the competitive adsorption of H_2O and NH_3 molecules on the acid sites [13]. After excluding H_2O from the reactant feed, the NO_x conversion at 300 °C was almost recovered. In addition, a slight decline in NO_x conversion occurred after the 150 ppm SO_2 was added for 1 h; then, the NO_x conversion became stable. After removing SO_2, the NO_x conversion was partially restored. However, the coexistence of 5.5% H_2O and 150 ppm SO_2 caused the NO_x conversion to decrease much more severely than when only 5.5% H_2O or 150 ppm SO_2 was used, which might be related to the deposition of ammonium sulfate on the surface of the catalyst which blocked the active sites [14]. However, the conversion was still maintained at a relatively high level

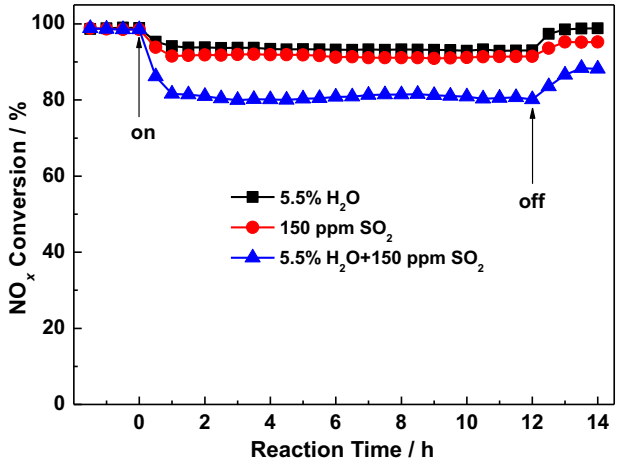

Fig. 3. NH_3–SCR activity over $Ce_1Ta_1O_x$ catalyst in the presence of H_2O/SO_2 at 300 °C under GHSV of 120, 000 mL g^{-1} h^{-1}.

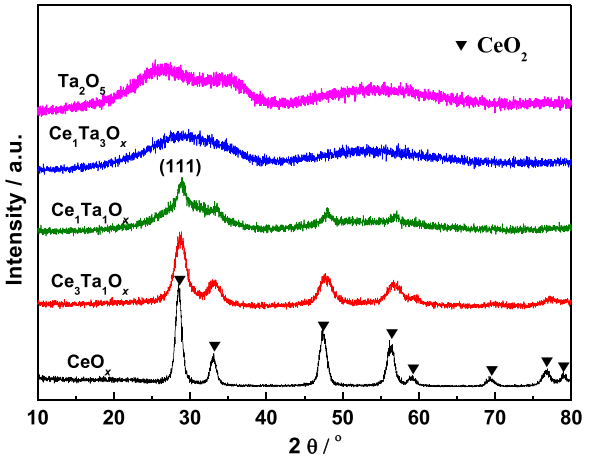

Fig. 4. XRD patterns of the $Ce_aTa_bO_x$ series catalysts.

with approximately 80% NO_x conversion attained during the measured period. The above results suggest that the $Ce_1Ta_1O_x$ catalyst has excellent H_2O and SO_2 durability, which is very competitive for practical applications in controlling NO_x emission.

3.3. Catalyst characterization

3.3.1. XRD results

The XRD patterns of $Ce_aTa_bO_x$ catalysts are shown in Fig. 4. The pristine CeO_x is present as cerianite (PDF# 43-1002). Similar patterns are observed for $Ce_3Ta_1O_x$ and $Ce_1Ta_1O_x$; whereas, full width at half maximum (FWHM) enlarges and the peak intensity decreases with the increase of Ta content. This can be attributed to a transformation of the bulk, regular crystals to an amorphous structure. Alternatively, it is possible that the number of crystal defection increases in smaller crystallites as the amount of doped-tantalum increased. Meanwhile, a slight shift toward higher 2θ value can be observed for all peaks, which might be attributed to the incorporation of Ta_2O_5 into CeO_x lattice. Ultimately, the average crystallite size of CeO_x decreases with FWHM being broadened and the increase of 2θ value (Table 1). However, no obvious peak is observed for $Ce_1Ta_3O_x$, suggesting a completely amorphous structure. The XRD pattern of the pristine Ta_2O_5 is also shown in Fig. 4. It is found that Ta_2O_5 calcined at 500 °C seems to be nearly amorphous. The reason is that the calcination temperature is lower than that necessary for the crystallization of Ta_2O_5 (750 °C) [15].

3.3.2. BET results

The BET surface areas of $Ce_aTa_bO_x$ catalysts prepared using different Ce/Ta ratios as well as their corresponding pore volumes and average pore diameters are provided in Table 1. With increasing Ta to Ce ratio, a marked increase in the BET surface area is observed, indicating that some synergistic effect must exist between the Ce and Ta oxide species. Meanwhile, larger S_{BET} could provide more surface active sites for the SCR reaction. The resulting high sur-

Table 1
Textual properties of the $Ce_aTa_bO_x$ series catalysts.

Samples	D^a (nm)	S_{BET} (m^2 g^{-1})	V_p (cm^3 g^{-1})	D_p (nm)
CeO_x	11.3	77.6	0.12	5.4
$Ce_3Ta_1O_x$	9.5	85.2	0.12	5.0
$Ce_1Ta_1O_x$	7.8	92.3	0.11	4.1
$Ce_1Ta_3O_x$	–	123.5	0.11	3.6
Ta_2O_5	–	71.8	0.20	9.9

[a] Crystallite size calculated by the Scherrer equation from the (1 1 1) reflection of CeO_2.

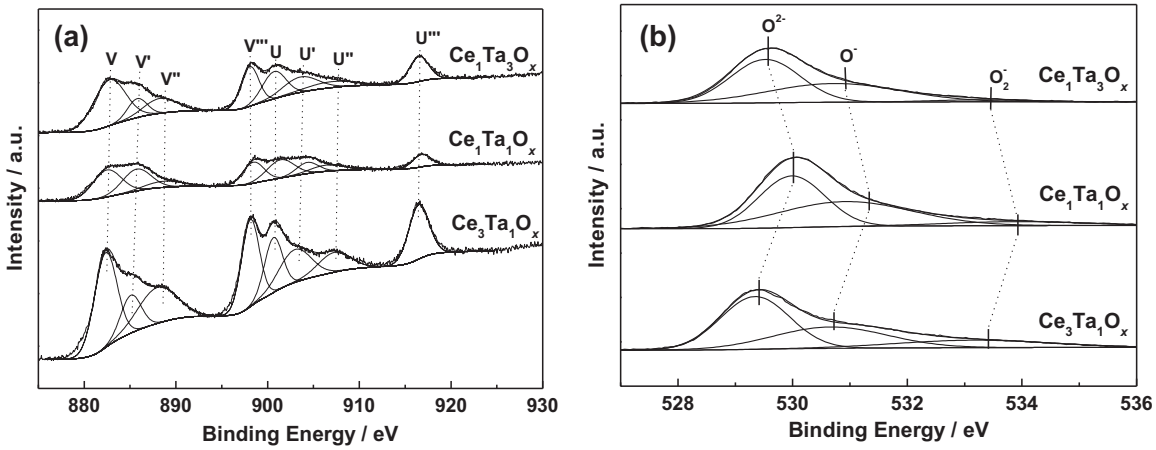

Fig. 5. XPS spectra of the $Ce_aTa_bO_x$ series catalysts over the spectral regions of Ce 3d (a) and (b) O 1s.

face area of $Ce_aTa_bO_x$ catalysts may be attributed to the inhibition of the individual crystallization during co-precipitation, as shown by XRD. Moreover, the amorphous structure usually has a higher surface area than the crystallized structure [5].

3.3.3. XPS results

To explore the chemical environment of Ce and Ta elements on the surface of the $Ce_aTa_bO_x$ catalysts, XPS spectra were measured. Fig. 5a depicts the Ce 3d spectra of the different samples. The four main $3d_{5/2}$ features appear at 881.7, 884.6, 888.1 and 897.7 eV corresponding to the V, V′, V″ and V‴ components, while the $3d_{3/2}$ features appear at 900.3, 902.7, 907.3 and 916.1 eV, corresponding to the U, U′, U″ and U‴ components, respectively [16]. The signals V′ and U′, characteristic of Ce^{3+}, evidently exist in the $Ce_aTa_bO_x$ catalysts [17]. The value of R^a (the Ce species ratio of Ce^{3+}/Ce^{4+}) increases from 0.233 ($Ce_3Ta_1O_x$) to 0.361 ($Ce_1Ta_1O_x$), as shown in Table 2. The increase in Ce^{3+} content is attributed to the interaction between cerium and the surrounding atoms, i.e., Ta, which leads to an increase in the oxygen vacancies and maintains cerium at the low-valence state. However, as the Ce/Ta molar ratio decreases to 1:3, the value of R^a drops to 0.218. These facts indicate that the Ce/Ta molar ratio being 1:1 maximizes the interaction between Ce and Ta.

As shown in Fig. 5b, the XPS of O 1s in $Ce_aTa_bO_x$ series catalysts were also recorded and deconvolved into three groups of sub-bands. The O 1s binding energies are located at 529.4–530.0, 530.7–531.3 and 533.3–533.9 eV, which are assigned to lattice oxygen species (O^{2-}) and chemisorbed oxygen species ($O_2^{\&-}$, containing O^- and O_2^-), respectively. The latter is often thought to be more reactive in oxidation reactions than the former due to its higher mobility, so many researchers have suggested that a high $O_2^{\&-}$ ratio is beneficial for the NO oxidation to NO_2 in the SCR reaction at low temperatures and thereafter facilitates the "fast SCR" reaction [10,18]. The relative concentration ratios of $O_2^{\&-}/O^{2-}$ for $Ce_aTa_bO_x$ catalysts were also calculated and the results are shown in Table 2. It is clear that $Ce_1Ta_1O_x$ has the greatest amount of chemisorbed oxygen species among the $Ce_aTa_bO_x$ catalysts, suggesting that the $Ce_1Ta_1O_x$ catalyst might have better activity for the oxidation of NO to NO_2 than $Ce_3Ta_1O_x$ and $Ce_1Ta_3O_x$ at low temperatures. As shown in Fig. S1a, at 150 °C, there is a good correlation between the pseudo-first order rate constant (k) and the relative concentration ratios of $O_2^{\&-}/O^{2-}$. Furthermore, the correlation is similarly good at 200 °C (Fig. S2a). The above results clearly indicate that the catalytic performances of the $Ce_aTa_bO_x$ catalysts at low temperatures are directly related to the relative concentration ratios of chemisorbed oxygen species ($O_2^{\&-}$). However, the low $O_2^{\&-}$ ratio over $Ce_1Ta_3O_x$ might favor the inhibition of the high-temperature oxidation of NH_3, which contributes to the NH_3–SCR activity at high temperatures. The results of the activity test for these catalysts were in agreement with this conclusion.

For tantalum-containing samples in Fig. S3, two well-defined peaks ascribed to $4f_{7/2}$ and $4f_{5/2}$ of Ta^{5+} are observed [19]. Concomitant with the change in CeO_x structure upon Ta concentration, the chemical state of Ta also changed with Ce concentration. The Ta $4f_{7/2}$ and $4f_{5/2}$ peaks shift from 26.0 to 27.9 eV in $Ce_3Ta_1O_x$ and 26.3 to 28.2 eV in $Ce_1Ta_3O_x$. Thus, the Ta and Ce metal cations influence each other to change their oxidation states on the surface of the $Ce_aTa_bO_x$ catalysts.

In addition, it is important to note that the O 1s XPS peak shift also suggests that Ce and Ta chemically interact with each other in the $Ce_aTa_bO_x$ mixed oxides. In other words, the mixed oxides are not simple mixtures of two different oxides but rather a composite in which Ce and Ta are subject to chemical interactions.

Table 2
XPS results, H_2 consumption and the ratios of Brønsted and Lewis acidities at 100 °C of the $Ce_aTa_bO_x$ series catalysts.

Samples	Ce species			O species				H_2 consumption (μmol)[c]	B/L[d]
	ce^{3+}	ce^{4+}	R^a	O^{2-}	O^-	O_2^-	R^b		
CeO_x	–	–	–	–	–	–	–	58.4	0.034
$Ce_3Ta_1O_x$	18.9	81.1	0.233	50.6	33.4	16.0	0.976	78.1	0.108
$Ce_1Ta_1O_x$	26.5	81.1	0.361	46.6	45.7	7.7	1.146	116.7	0.526
$Ce_1Ta_3O_x$	17.9	82.1	0.218	53.1	43.7	3.2	0.883	64.9	1.721
Ta_2O_5	–	–	–	–	–	–	–	–	2.525

[a] Determined by the Ce species ratio of the Ce^{3+}/Ce^{4+}.
[b] Determined by the oxygen species ratio of the adsorbed oxygen ($O_2^- + O^-$)/lattice oxygen (O^{2-}).
[c] The amount of H_2 consumption below 700 °C was quantified by CuO used as a calibration reference.
[d] The ratios of Brønsted and Lewis acidities were obtained by calculating the integrated peak areas of 1436 and 1127 (1220) cm^{-1} in Fig. 7.

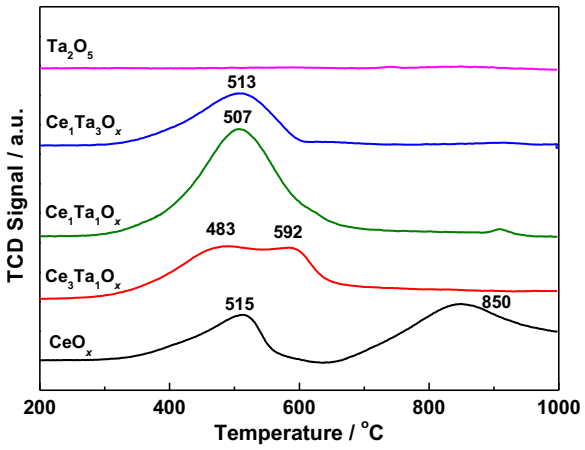

Fig. 6. H_2-TPR profiles of the $Ce_aTa_bO_x$ series catalysts.

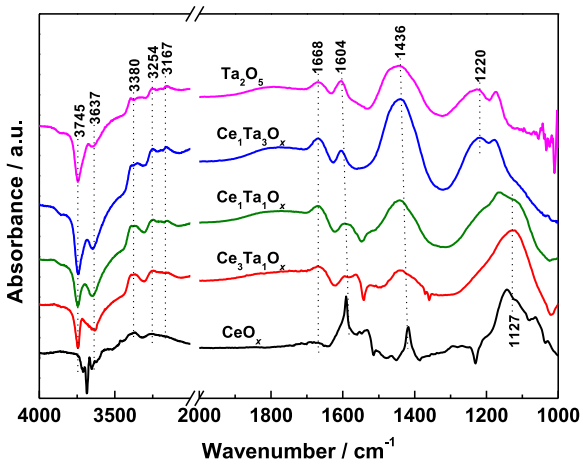

Fig. 7. DRIFTS spectra of the NH_3 desorption of the $Ce_1Ta_1O_x$ catalyst at the temperature range of 100–350 °C.

3.3.4. H_2-TPR results

For metal oxide catalysts, H_2-TPR measurement can simultaneously reflect the reducibility of a metallic ion with high valence, converting it to an ion with low valence or metallic atom, and the potential to remove or take up oxygen, i.e., the mobility of the lattice oxygen (O^{2-}) [20]. Thus, the temperature of reduction peak is taken as a measure to evaluate the redox ability of catalyst. The results of H_2-TPR analysis for $Ce_aTa_bO_x$ catalysts are shown in Fig. 6. The pristine Ta_2O_5 does not show any obvious reduction peak in the whole temperature range. Therefore, all H_2 consumption peaks that occurred over other samples could be attributed to the reduction of cerium species. The pristine CeO_x shows two apparent reduction peaks centered at 515 and 850 °C, which can be assigned to the reduction of surface Ce^{4+} to Ce^{3+} and bulk Ce^{4+} (to Ce^{3+}), respectively [21–23]. However, $Ce_aTa_bO_x$ only shows apparent reduction peaks ranging from 400 to 600 °C, and an obvious shift toward lower temperatures is observed for the high-temperature peak with Ta addition. In general, the nucleation and contracting sphere models are used to explain the process of H_2-TPR [24]. Whichever model we choose, the reduction of oxide occurred first on the surface and then progressively affects the bulk. When the surface oxide and hydrogen came into contact, the reaction started and after some time, the oxide grain was totally covered by a layer of metal product, which formed in the first instant of the reaction. From this moment a decrease of the reaction interface began because of the overlapping of the metal product as well as the reaction rate. Therefore, the reduction of the oxide grains inside the crystallite (bulk oxide) became even more difficult. If the crystallite size reduced, this process might continue more easily than ever before. Trovarelli et al. have found that CeO_x reduction at high temperatures is strongly depended on its crystallite size, an obvious shift toward lower temperatures was observed for the high-temperature peak by reducing CeO_x crystallite size [25]. The results of XRD showed that the average crystallite size of CeO_x decreases with addition of Ta. Moreover, a strong interaction between Ce and Ta evidenced by XPS could further improve the redox properties of CeO_x.

Yao and Yao found that the catalytic performance of the ceria-based catalyst is mainly related to the H_2 consumption peaks below 700 °C, which can be associated with the reduction of surface capping oxygen [26]. Johnson and Mooi have confirmed the qualitative relationship between the observed quantity of hydrogen consumed in reducing chemisorbed oxygen species and BET surface areas of the cerium specimens [27]. Thus, we calculated both the total H_2 consumption for the peaks below 700 °C (Table 2) and the H_2 consumption (<700 °C) per specific surface area (H_2/S_{BET}) over the $Ce_aTa_bO_x$ series catalysts. It is noteworthy that the amount of H_2 consumption for the peaks below 700 °C on the $Ce_1Ta_1O_x$ catalyst is the largest, which is 116.7 μmol. In addition, a good correlation between the value of H_2/S_{BET} and the relative concentration ratios of $O_2^{\&-}/O^{2-}$ can be observed (Fig. S1b). This is further proof that the H_2 consumption peaks below 700 °C are indeed associated with the reduction of surface capping oxygen over the $Ce_aTa_bO_x$ series catalysts. Moreover, it can also be found that a good correlation between the value of k and H_2/S_{BET} at 150 and 200 °C (Fig. S1c and S2b).

3.3.5. The results of DRIFTS spectra of NH_3 adsorption and NH_3-TPD

The presence of surface acid sites on the catalyst and their acidity can be determined using NH_3. This information is obtained by studying the DRIFTS spectra of the adsorbed NH_3. The DRIFTS spectra of the adsorbed NH_3 on the $Ce_aTa_bO_x$ series catalysts at 100 °C are shown in Fig. 7. The bands at 1604 and 1127 (1220) cm^{-1} are assigned to asymmetric and symmetric bending vibrations of the N—H bonds in NH_3 coordinately linked to Lewis acid sites, whereas the bands at 1436 and 1668 cm^{-1} were attributed to asymmetric and symmetric bending vibrations of NH_4^+ species on Brønsted acid sites [28]. In the N—H stretching vibration region of coordinated NH_3, the bands were found at 3167, 3254 and 3380 cm^{-1} [29]. The negative bands at approximately 3637 and 3745 cm^{-1} were also found, which could be ascribed to surface O—H stretching [30]. The ratios of Brønsted and Lewis acidities were obtained by calculating the integrated peak areas of 1436 and 1127 (1220) cm^{-1} in the DRIFTS spectra at 100 °C, and the results are listed in Table 2. For the CeO_x catalyst, few Brønsted acid sites were detected, consistent with the results in published literature [8,9]. However, the introduction of Ta to CeO_x results in more Brønsted acid sites on the catalyst surface, and the ratios of B/L increase in parallel with the amount of Ta added. The increased Brønsted acid sites are mainly composed of Ta—OH sites arising from partially hydrated tantalum species, such as Ta=O, Ta—O—Ta, and Ce—Ta—O.

Fig. 8 shows the NH_3 desorption from Lewis and Brønsted acid sites on $Ce_1Ta_1O_x$ in the temperature range of 100–350 °C. The intensities of all of the bands decrease when the temperature increases, indicating that the ammonia molecules have desorbed. The IR bands of NH_4^+ ions (1436 and 1668 cm^{-1}) almost disappear at 250 °C, while the coordinated NH_3 (1220 and 1604 cm^{-1}) are still detected at 300 °C in N_2. Therefore, the coordinated NH_3 on Lewis acidic sites are much more stable at high temperatures than the NH_4^+ species on the Brønsted acidic sites.

Fig. 9 shows the NH_3-TPD profiles for ammonia adsorption on the $Ce_aTa_bO_x$ series catalysts at 100 °C. A large peak including three

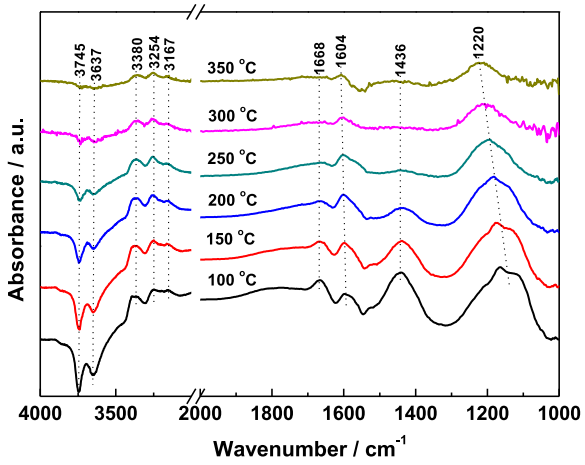

Fig. 8. DRIFTS spectra of the NH_3 adsorption of the $Ce_aTa_bO_x$ series catalysts at 100 °C.

main ammonia desorption peaks is observed over the entire desorption temperature range. Two large ammonia desorption peaks are located at 204–215 and 257–321 °C, and a small peak is located at 153–172 °C. According to the above IR results, the intensity of the ammonia peak on both the Lewis and Brønsted acid sites slightly decreased between 100 and 200 °C; the intensity of the ammonia adsorption peak on Brønsted acid sites completely disappeared, while the peak associated with Lewis acidic sites decreased between 200 and 300 °C. Furthermore, only the ammonia adsorbed on the Lewis acidic sites was reduced at temperatures above 300 °C. Therefore, the peak at 153–172 °C should be assigned to the physically adsorbed NH_3 because these species generated a free NH_3 signal in the IR spectra. Meanwhile, the peak at 204–215 °C is assigned to ammonia adsorbed on the acid sites, including weakly and strongly bound NH_3 species (e.g., ammonia adsorbed on Lewis and Brønsted acid sites); the peak at 257–321 °C is assigned to the ammonia strongly adsorbed on the Lewis acid sites.

Combined with the results of DRIFTS spectra of NH_3 adsorption and NH_3-TPD experiments, we find that Ta addition could

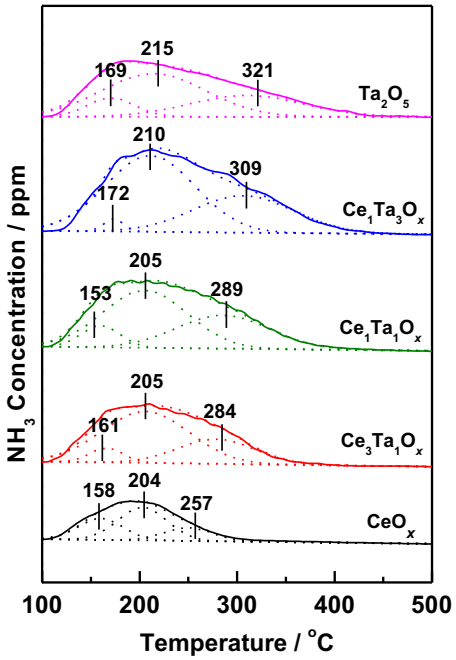

Fig. 9. NH_3-TPD curves of the $Ce_aTa_bO_x$ series catalysts.

increase the number of Brønsted acid sites on the catalyst surface, that is, more surface O—H groups are formed in the presence of Ta. Furthermore, the coordinated NH_3 on the Lewis acidic sites are much more stable at high temperatures than the NH_4^+ species on the Brønsted acidic sites. Numerous studies have shown that both Brønsted acid and Lewis acid sites can contribute to the NH_3–SCR reaction [8,9,31]. Thus, it might be concluded that the NH_4^+ species at Brønsted acid sites mainly contribute to the reaction only at relatively low temperatures due to their lower thermal stability, whereas the coordinated NH_3 at Lewis acid sites, which have better thermal stability, contribute to the SCR activity of $Ce_aTa_bO_x$ catalysts at both low and high temperatures.

3.3.6. *The results of DRIFTS spectra of NO_x adsorption and $NO + O_2$-TPD*

To acquire information regarding different NO_x adsorbed species, the NO_x adsorption properties over the $Ce_aTa_bO_x$ series catalysts at 100 °C were also tested using in situ DRIFTS, and the results are shown in Fig. 10a. The bands centered at 1242 and 1601 cm^{-1} can be ascribed to the presence of bridging nitrate. The bands at 1436, 1459, 1532 and 1576 cm^{-1} are assigned to M-NO_2 nitro compounds, monodentate nitrite, monodentate nitrate and bidentate nitrate, respectively [5,24,32]. The band at 1625 cm^{-1} can be attributed to the adsorbed NO_2 [24]. Furthermore, the bands attributed to nitrite and nitrate species on $Ce_aTa_bO_x$ series catalysts are deconvoluted into several groups of sub-bands as shown in Fig. 1b. The integral areas are calculated accordingly, which can represent the adsorption amounts of different nitrite and nitrate species at 100 °C. And then, the integral areas as a function of $Ce_aTa_bO_x$ series catalysts are depicted in Fig. 10c. As shown in Fig. 10c, the intensities of all bands increase with Ta addition, except the band at 1436 cm^{-1}. However, with increasing Ta doping, the intensities of the bands (1242 and 1601 cm^{-1}) attributed to bridging nitrate decrease, as well as the band (1576 cm^{-1}) assigned to bidentate nitrate (Fig. 10a and c). In conclusion, it can be concluded that Ta addition can promote the presence of nitrite and nitrate species.

Fig. 11 shows the DRIFTS spectra of $NO + O_2$ on $Ce_1Ta_1O_x$ in the temperature range of 100–350 °C. The intensities of the bands assigned to monodentate nitrite, monodentate nitrate, bridging nitrate and adsorbed NO_2 content decrease with increasing temperature, whereas the intensity of the band ascribed to bidentate nitrate exhibits a slight increase in the range of 100–200 °C and then a significant decrease at 200 °C and higher temperatures. These findings indicate that the variation from bridging nitrate into a bidentate nitrate happened at low temperatures. Meanwhile, it can be found that the bridging and bidentate nitrates remain adsorbed on the catalyst in a relative thermal stability form until approximately 350 °C. In contrast, monodentate nitrite and monodentate nitrate can hardly be observed at high temperatures (≥250 °C).

Furthermore, $NO + O_2$-TPD experiments are conducted to study the oxidation activity for the conversion of NO to NO_2 on the $Ce_aTa_bO_x$ series catalysts and the results are shown in Fig. 12. It can easily be seen that $Ce_1Ta_1O_x$ desorbs much more NO_2 than other samples. The XPS results have shown that $Ce_1Ta_1O_x$ had the most Ce^{3+} state, which could create a charge imbalance in the vacancies and unsaturated chemical bonds over the catalyst surface, after which more NO could be easily oxidized into NO_2. The process of NO oxidation to NO_2, subsequently forming the surface nitrate and adsorbed NO_2 species, is crucial during the NH_3–SCR reaction. However, the influences of the thermal stability of nitrate species must be considered. The weak bonding of NO_2 at relatively low temperatures may enhance the activity by facilitating the "fast SCR" reaction, whereas the desorption of NO_2 at higher temperatures, which could be ascribed to the decomposition of the strongly bound nitrate species (the bridging and bidentate nitrates),

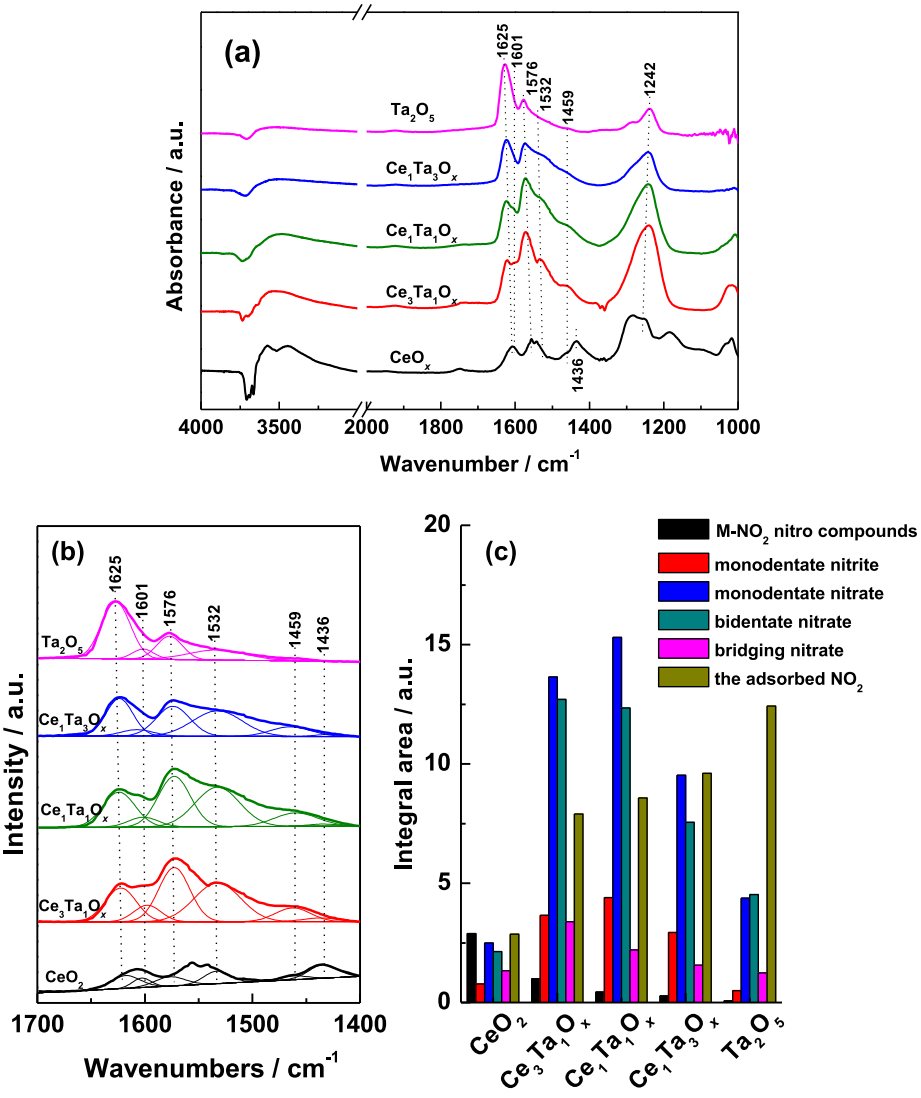

Fig. 10. DRIFTS spectra of the NO_x adsorption of the $Ce_aTa_bO_x$ series catalysts at 100 °C (a). Deconvoluted results of bands attributed to nitrite and nitrate species (b). Correlation between amounts of relevant nitrite and nitrate species and the $Ce_aTa_bO_x$ series catalysts (c).

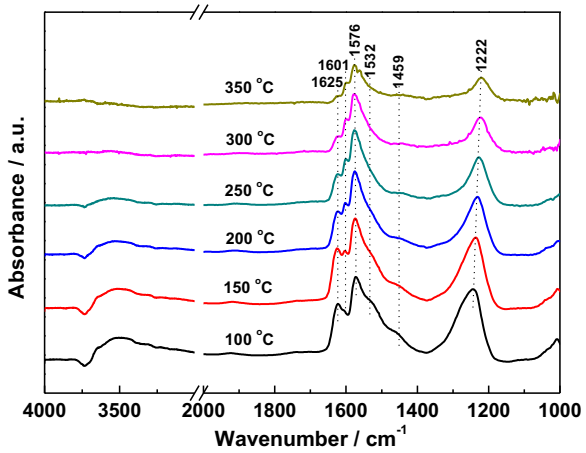

Fig. 11. DRIFTS spectra of the NO_x desorption of the $Ce_1Ta_1O_x$ catalyst at the temperature range of 100–350 °C.

results in increased thermal stability. Increased thermal stability is unfavorable to the SCR reaction that results from occupying the active sites of the catalysts at low temperatures. In addition, it is noted that the $Ce_1Ta_3O_x$ sample shows almost no NO_2 peak; however, the activity at low temperatures is quite high compare to CeO_x samples. This can be explained as follows: At low temperatures, most researchers believe that NH_3 is firstly adsorbed to acid center, and then react with aerial NO through E-R mechanism [33] or adsorbed NO_x species through L-H mechanism [34]. Our DRIFTS results showed that the NH_3 species bonded to both Brønsted and Lewis acid sites could participate in the SCR reaction with monodentate nitrite and adsorbed NO_2 species at low temperatures. Thus, the acidity is one of the important parameters that determine the extent of NO_x reduction with NH_3 over $Ce_aTa_bO_x$ catalysts. As shown in Fig. 9, it can be seen that the acidity amount of the $Ce_1Ta_3O_x$ catalyst is much more than that of CeO_x. Although $Ce_1Ta_3O_x$ is unable to oxidize NO into NO_2 in quantity, the SCR reaction can occur between the adsorbed NH_3 and monodentate nitrite. While, CeO_x exhibited poor catalytic activity due to its insufficient acidity amount. However, this is not to say that the NO oxidation to NO_2 is unimportant. If a series of catalysts has the similar acidity amount, the presence of NO_2 can promote the occurrence of the

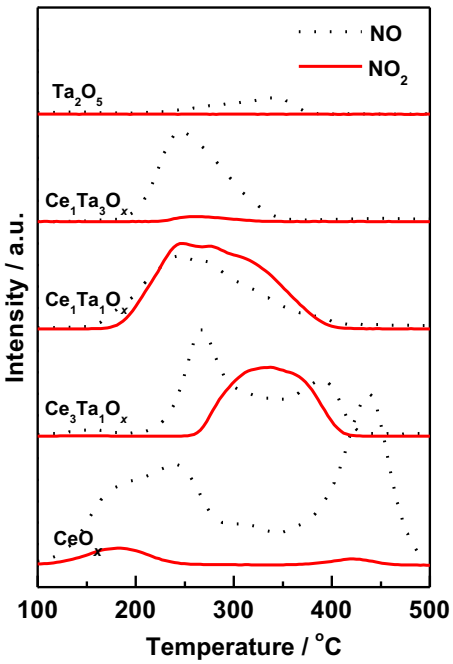

Fig. 12. $NO + O_2$-TPD curves of the $Ce_aTa_bO_x$ series catalysts.

"fast SCR" reaction over the catalyst and enhance the activity of the catalyst at low temperatures. For instance, the $Ce_1Ta_1O_x$ catalyst showed better catalytic performance than $Ce_3Ta_1O_x$, $Ce_1Ta_3O_x$ and Ta_2O_5.

3.4. Reactivity of surface-adsorbed species

Extensive studies on the reactivity of surface-adsorbed NH_3 and NO_x species were carried out using in situ DRIFTS over the $Ce_1Ta_1O_x$ catalyst at 200 and 350 °C, respectively (Fig. 13). Fig. 13a shows the DRIFTS spectra of $Ce_1Ta_1O_x$ catalyst in a flow of $NO + O_2$ after the catalyst was pre-exposed to a flow of NH_3 for 30 min followed by N_2 purging for 30 min at 200 °C. As illustrated in Fig. 13a, switching the gas to $NO + O_2$ led to a decrease of the intensities of all bands assigned to NH_3 species bonded to Lewis and Brønsted acid sites (1194, 1433, 1604, 1668, 3157, 3256 and 3372 cm^{-1}), and these bands vanished in 7 min. Meanwhile, some new bands attributed to NO_x species appeared (1236, 1455, 1537, 1572 and 1605 cm^{-1}). This observation indicates that the NH_3 species bonded to both Lewis and Brønsted acid sites can participate in the SCR reaction at 200 °C. When the gaseous order was reversed, switching the gas to NH_3 led to the decrease of the intensities of adsorbed NO_2 (1621 cm^{-1}) and monodentate nitrite (1455 cm^{-1}) bands. These bands vanished in 5 min, indicating that these species are reactive in the NH_3–SCR process. Meanwhile, the amount of other nitrate species decreases slightly. Simultaneously, the bands ascribed to the adsorbed NH_3 species appeared. The above results show that the NH_3 species bonded to both Brønsted and Lewis acid sites can participate in the

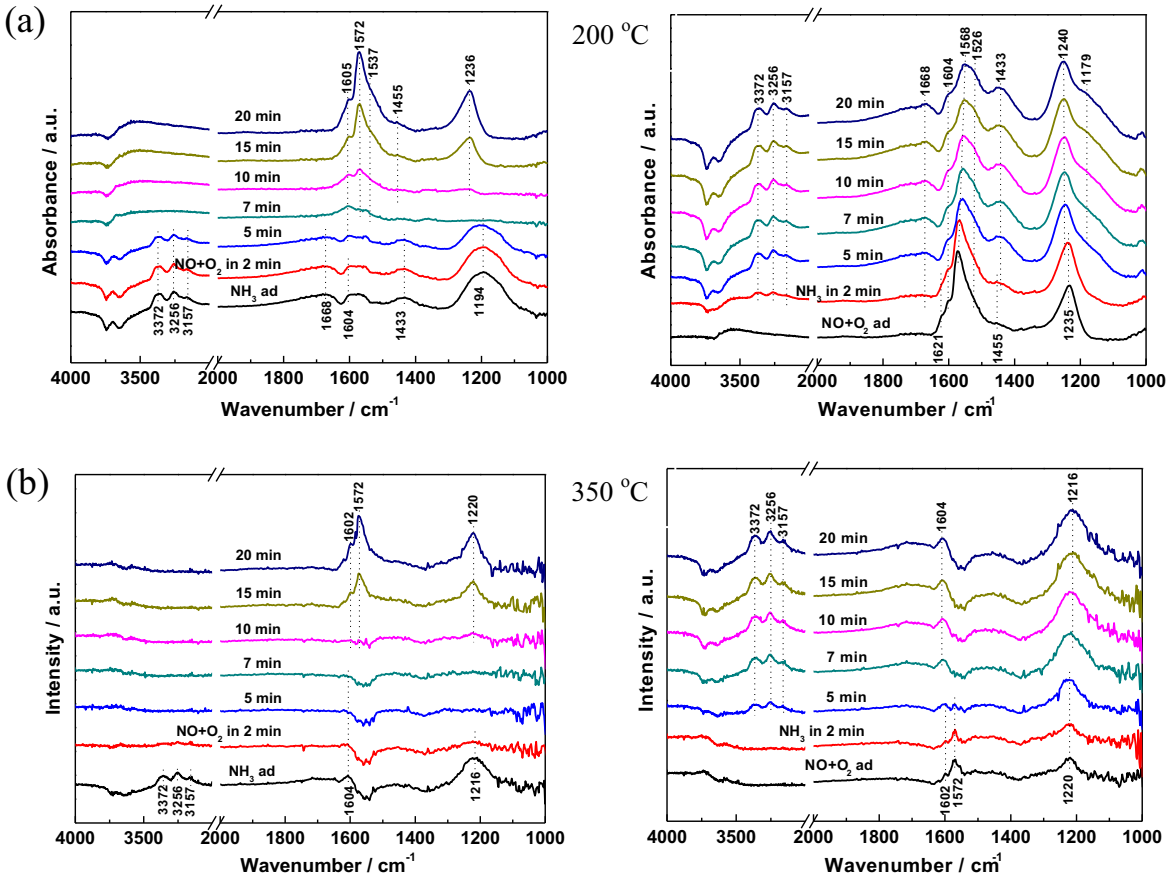

Fig. 13. Sequential DRIFTS spectra of $Ce_1Ta_1O_x$ recorded under various atmospheres: the dehydrated catalyst was first treated by NH_3, then $NO + O_2$ was added and the reversed order at (a) 150 °C and (b) 350 °C.

SCR reaction with monodentate nitrite and adsorbed NO_2 species at low temperatures.

Fig. 13b presents the DRIFTS spectra of $Ce_1Ta_1O_x$ catalyst in a flow of NO + O_2 after the catalyst was pre-exposed to a flow of NH_3 for 30 min followed by N_2 purging for 30 min at 350 °C. After the catalyst exposed to NH_3, only the coordinated NH_3 on the Lewis acid sites (1226 and 1604 cm^{-1}) could be detected. Bridging and bidentate nitrate species (1220, 1602 and 1572 cm^{-1}) emerged when NO and O_2 were introduced. When the gas order was reversed, all of the adsorbed NO_x species decreased when switching the gas to NH_3. After 7 min, only the coordinated NH_3 on the Lewis acid sites could be observed in the DRIFT spectra. The results indicate that at high temperatures, even thermally stable bridging and bidentate nitrate species can react with the coordinated NH_3 on the Lewis acid sites.

4. Conclusions

In conclusion, the novel $Ce_aTa_bO_x$ series catalysts prepared by co-precipitation method presented superior NH_3–SCR activity and N_2 selectivity over a relatively wide temperature range. Moreover, the $Ce_1Ta_1O_x$ catalyst displayed good resistance to H_2O and SO_2, which is very promising for practical applications in controlling NO_x emissions.

Ta addition could decrease the average crystallite size of CeO_x, and thus increase the BET surface area of the catalysts, which could provide more active sites for the NH_3–SCR reaction. The results of XPS indicated that a much strong interaction happened between Ce and Ta for the increased appearance of Ce^{3+} and chemisorbed oxygen species ($O_2^{\&-}$, containing O^- and O_2^-). These oxygen species are beneficial for the NO oxidation to NO_2 in the SCR reaction at low temperatures and thereafter facilitate the “fast SCR” reaction.

The results of H_2-TPR showed that Ta addition influenced the reducibility of the catalysts. The DRIFTS spectra of NH_3 adsorption and NH_3-TPD indicated that Ta addition increased the surface acidity of the catalysts, especially the number of Brønsted acid sites, which are key acid sites at low temperatures. Ta addition also promoted the presence of nitrite and nitrite species. Among them, monodentate nitrite and the adsorbed NO_2 favor the SCR reaction at low temperatures.

Finally, the $Ce_1Ta_1O_x$ catalyst was used to study the reactivity of surface-adsorbed NH_3 and NO_x species by in situ DRIFTS. At low temperatures, the NH_3 species bonded to both Brønsted and Lewis acid sites can participate in the SCR reaction with monodentate nitrite and adsorbed NO_2 species. By contrast, at high temperatures, only the coordinated NH_3 on the Lewis acid sites can be observed on the DRIFTS spectra, while bridging and bidentate nitrate species are active.

Acknowledgements

This work was financially supported by the National Natural Science Fund of China (Grant Nos. 21325731, 51478241 and 21221004) and the National High-Tech Research and Development (863) Program of China (Grant No. 2013AA065401, 2013AA065304).

Appendix A. Supplementary data

Supplementary data associated with this article can be found, in the online version, at http://dx.doi.org/10.1016/j.apcatb.2015.04.023.

References

[1] H. Bosch, F. Janssen, Catal. Today 2 (1988) 369–379.
[2] N.Y. Topsøe, Science 265 (1994) 1217–1219.
[3] G.S. Qi, R.T. Yang, Chem. Commun. (2003) 848–849.
[4] F. Li, Y. Zhang, D. Xiao, D. Wang, X. Pan, X. Yang, ChemCatChem 2 (2010) 1416–1419.
[5] P. Li, Y. Xin, Q. Li, Z. Wang, Z. Zhang, L. Zheng, Environ. Sci. Technol. 46 (2012) 9600–9605.
[6] L. Chen, J. Li, W. Ablikim, J. Wang, H. Chang, L. Ma, J. Xu, M. Ge, H. Arandiyan, Catal. Lett. 141 (2011) 1859–1864.
[7] W. Shan, F. Liu, H. He, X. Shi, C. Zhang, Chem. Commun. 47 (2011) 8046–8048.
[8] Y. Peng, R. Qu, X. Zhang, J. Li, Chem. Commun. 49 (2013) 6215–6217.
[9] R. Qu, X. Gao, K.J. Li, Appl. Catal. B 142–143 (2013) 290–297.
[10] W. Shan, F. Liu, H. He, X. Shi, C. Zhang, Appl. Catal. B 115–116 (2012) 100–106.
[11] Z. Liu, Y. Yi, J. Li, S.I. Woo, B. Wang, X. Cao, Z. Li, Chem. Commun. 49 (2013) 7726–7728.
[12] Z. Liu, J. Zhu, J. Li, L. Ma, S.I. Woo, ACS Appl. Mater. Interface 6 (2014) 14500–14508.
[13] G. Busca, L. Lietti, G. Ramis, F. Berti, Appl. Catal. B 18 (1998) 1–36.
[14] F. Liu, K. Asakura, H. He, W. Shan, X. Shi, C. Zhang, Appl. Catal. B 103 (2011) 369–377.
[15] T. Ushikubo, K. Wada, Appl. Catal. 67 (1990) 25–38.
[16] E. Bêche, P. Charvin, D. Perarnau, S. Abanades, G. Flamant, Surf. Interface Anal. 40 (2008) 264–267.
[17] M.M. Natile, A. Glisenti, Chem. Mater. 17 (2005) 3403–3414.
[18] L. Chen, J. Li, M. Ge, J. Phys. Chem. C 113 (2009) 21177–21184.
[19] H. Szymanowski, O. Zabeida, J.E. Klemberg-Sapieha, L. Martinu, J. Vac. Sci. Technol. A 23 (2005) 241–247.
[20] Z. Zhao, Y. Yamada, A. Ueda, H. Sakurai, T. Kobayashi, Catal. Today 93 (2004) 163–171.
[21] G. Neri, A. Pistone, C. Milone, S. Galvagno, Appl. Catal. B 38 (2002) 321–329.
[22] S.M. Lee, S.C. Hong, Appl. Catal. B 163 (2015) 30–39.
[23] L. Zhang, L. Li, Y. Cao, X. Yao, C. Ge, F. Gao, Y. Deng, C. Tang, L. Dong, Appl. Catal. B 165 (2015) 589–598.
[24] N.W. Hurst, S.J. Gentry, A. Jones, Catal. Rev. 24 (1982) 233–309.
[25] A. Trovarelli, C. Deleitenburg, G. Dolcetti, J.L. Lorca, J. Catal. 151 (1995) 111–124.
[26] H.C. Yao, Y.F. Yu Yao, J. Catal. 86 (1984) 254–265.
[27] M.F.L. Johnson, J. Mooi, J. Catal. 103 (1987) 502–505.
[28] K.I. Hadjiivanov, Catal. Rev. 42 (2000) 71–144.
[29] A.S. Mamede, E. Payen, P. Grange, G. Poncelet, A. Ion, M. Alifanti, V.I. Pârvulescu, J. Catal. 223 (2004) 1–12.
[30] F. Liu, H. He, Y. Ding, C. Zhang, Appl. Catal. B 93 (2009) 194–204.
[31] A. Vittadini, M. Casarin, A. Selloni, J. Phys. Chem. B 109 (2005) 1652–1655.
[32] L. Chen, J. Li, M. Ge, Environ. Sci. Technol. 44 (2010) 9590–9596.
[33] F. Eigenmann, M. Maciejewski, A. Baiker, Appl. Catal. B 62 (2006) 311–318.
[34] W.S. Kijlstra, D.S. Brands, H.I. Smit, E.K. Poels, A. Bliek, J. Catal. 171 (1997) 219–230.